

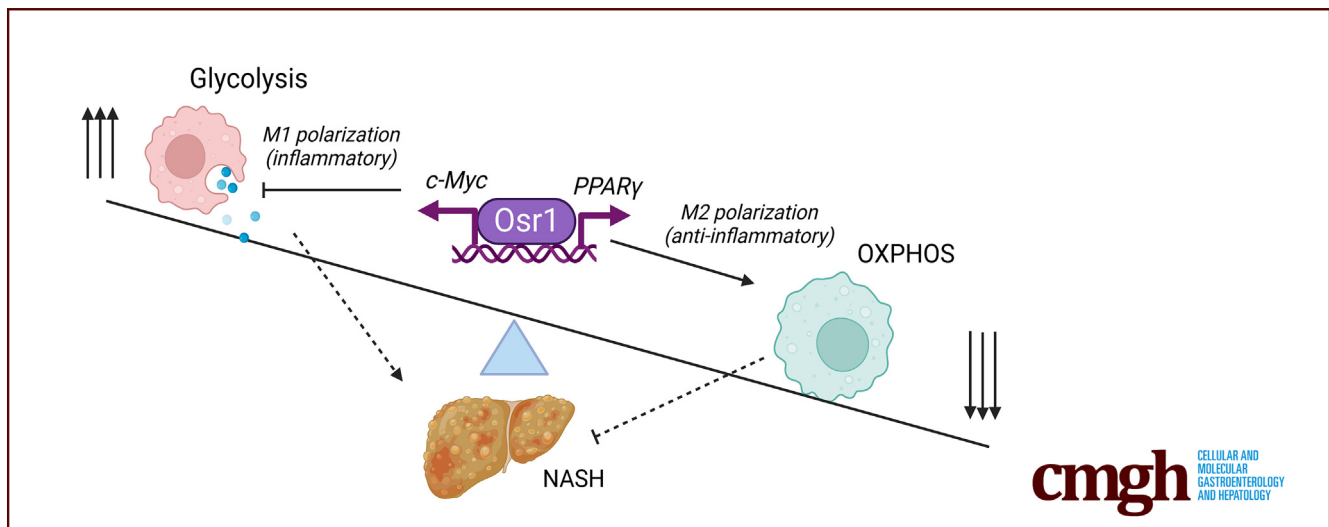
ORIGINAL RESEARCH

Osr1 Regulates Macrophage-mediated Liver Inflammation in Nonalcoholic Fatty Liver Disease Progression



Lin Liu,¹ Yi Zhou,² Zhimin Liu,¹ Jianguan Li,^{3,6} Linghao Hu,⁴ Leya He,¹ Guannan Gao,^{3,6} Brian Kidd,^{3,6} Alexandra Walsh,⁴ Rulang Jiang,⁵ Chaodong Wu,¹ Ke Zhang,^{1,6} and Linglin Xie¹

¹Department of Nutrition, Texas A&M University, College Station, Texas; ²Tongji Hospital, Huazhong University of Science and Technology, Wuhan, Hubei, China; ³Department of Statistics, Texas A&M University, College Station, Texas; ⁴Department of Biomedical Engineering, Texas A&M University, College Station, Texas; ⁵Division of Developmental Biology, Cincinnati Children's Hospital Medical Center, Cincinnati, Ohio; and ⁶Institute of Biosciences & Technology, Texas A&M University, Houston, Texas



SUMMARY

Osr1 regulates macrophage-mediated liver inflammation during nonalcoholic steatohepatitis development by modulating cell polarization and metabolisms. Targeting macrophage Osr1 can be a promising treatment strategy for nonalcoholic steatohepatitis.

BACKGROUND & AIMS: Liver macrophage-mediated inflammation contributes to the pathogenesis of the nonalcoholic fatty liver disease (NAFLD) and nonalcoholic steatohepatitis (NASH). Odd skipped-related 1 (Osr1) is a putative transcription factor previously reported to be involved in NASH progression; however, the underlying mechanisms remain unknown. The current study focused on the role of Osr1 in macrophage polarization and metabolism and its associated functions in the inflammation-induced pathogenesis of NASH.

METHODS: OSR1/Osr1 expression patterns were compared in normal and NASH patients and mouse livers. NASH was established and compared between hepatocyte-specific Osr1 knockout (*Osr1^{ΔHep}*), macrophage-specific Osr1 knockout (*Osr1^{ΔMφ}*), and wild-type (*Osr1^F*) mice fed with 3 different

chronic obesogenic diets and methionine choline-deficient diet. Using genetic and therapeutic strategies in vitro and in vivo, the downstream targets of Osr1 and the associated mechanisms in inflammation-induced NASH were established.

RESULTS: Osr1 was expressed in both hepatocytes and macrophages and exhibited different expression patterns in NASH. In NAFLD and NASH murine models, deleting *Osr1* in myeloid cells (*Osr1^{ΔMφ}*), but not hepatocytes, aggravated steatohepatitis with pronounced liver inflammation. Myeloid Osr1 deletion resulted in a polarization switch toward a pro-inflammatory phenotype associated with reduced oxidative phosphorylation activity. These inflamed *Osr1^{ΔMφ}* macrophages promoted steatosis and inflammation in hepatocytes via cytokine secretion. We identified 2 downstream transcriptional targets of Osr1, *c-Myc*, and *PPARγ* and established the Osr1-PPARγ cascade in macrophage polarization and liver inflammation by genetic study and rosiglitazone treatment in vivo. We tested a promising intervention strategy targeting Osr1-PPARγ by AAV8L-delivered Osr1 expression or rosiglitazone that significantly repressed NAFLD/NASH progression in *Osr1^F* and *Osr1^{ΔMφ}* mice.

CONCLUSIONS: Myeloid Osr1 mediates liver immune homeostasis and disrupting Osr1 aggravates the progression of

NAFLD/NASH. (*Cell Mol Gastroenterol Hepatol* 2023;15:1117–1133; <https://doi.org/10.1016/j.jcmgh.2022.12.010>)

Keywords: Inflammation; Macrophages; Metabolism; NASH; Osr1.

Nonalcoholic fatty liver disease (NAFLD) is associated with metabolic syndrome, diabetes, obesity, and hyperlipidemia; it has become one of the most common chronic liver diseases, affecting around 25% of the global population.^{1,2} One-third of NAFLD develops into a more inflammatory subtype, nonalcoholic steatohepatitis (NASH), characterized by hepatic inflammation and steatosis with or without fibrosis.³ More recent analyses show an overall NASH prevalence of 59% in NAFLD-biopsied patients.⁴ Among those without an NAFLD diagnosis, 3% to 5% of all adults are estimated to have NASH.⁵ The classic “2-hit” hypothesis proposed that lipotoxicity-induced oxidative stress, endoplasmic reticulum stress, and increased inflammation drive hepatic injury in NASH.⁶ Immune imbalance accompanied by dietary and metabolic factors and genetic susceptibility contribute to NAFLD pathogenesis. The increasingly accepted “multiple parallel hit” model considers environmental factors, genetic and epigenetic influences, and variations in the crosstalk between multiple tissues and organs.⁷ In both theories, inflammation involving macrophage actions is the central mechanism, suggesting targeting macrophages for promising therapeutic strategies.

In the liver, macrophages are classified into 2 major subsets, liver-resident Kupffer cells (KCs) and recruited monocyte-derived macrophages from peripheral blood. Following hepatic injury, KCs recruit additional monocytes that undergo macrophage metabolic reprogramming correlated with their functional state. Although several subpopulations were identified during liver injury, the classical M1/M2 theory remains fundamental. In high-fat diet (HFD) and or methionine- and choline-deficient diet (MCD)-fed mice, there is macrophage infiltration with a dominant M1 phenotype that relies on glycolysis to sustain phagocytic activity and cytokine production; the result is pronounced inflammation-induced hepatic injury.⁸ Differentiation toward alternatively activated macrophages (M2 type), dependent on oxidative phosphorylation (OXPHOS) and fatty acid oxidation (FAO),⁹ is associated with hepatic injury attenuation and improved insulin sensitivity.¹⁰ These findings suggest that targeting macrophage metabolism is a promising way to address macrophage-associated inflammation. Nevertheless, it remains unclear how macrophage metabolism is regulated to alter macrophage polarization (or vice versa), contributing to NASH pathophysiology.

Odd skipped-related 1 (Osr1) encodes a putative transcription factor containing 4 C2H2-type zinc finger motifs.¹¹ *Osr1* was essential for developing significant organs in a murine model, including the heart, lung, and kidney.^{12,13} *Osr1* is a tumor suppressor gene and a potential prognostic biomarker in many cancers.^{14–16} We recently reported that *Osr1* is involved in NAFLD progression.^{17,18}

Osr1^{+/-} mice displayed liver injury during NAFLD induction with overactivated JNK and NF-κB signaling and elevated hepatic expression levels of pro-inflammatory cytokine genes. The current study investigated the cell-specific role of *Osr1* in macrophage polarization and metabolism, providing a better mechanistic understanding of how macrophage-associated inflammation drives NASH progression.

Results

OSR1/Osr1 was Highly Expressed in Macrophages During NASH


The expression pattern of OSR1/*Osr1* was examined in the liver tissues of humans and mice. In humans, strong OSR1 expression was observed in several cell types in healthy livers (Figure 1A). Hepatocyte OSR1 expression was predominantly found in the cytosol, which formed clusters (Figure 1A). By contrast, expression of OSR1 in non-parenchymal cells (NPCs) was observed in the nucleus (Figure 1A, green arrow). Interestingly, although OSR1 staining in the NASH liver was significantly reduced in the hepatocytes, it was maintained in the NPCs of increased numbers (Figure 1A, red arrow).

In the mouse liver, the expression pattern of *Osr1* was similar to that of the human liver. In the NASH liver, *Osr1* expression was significantly decreased in the hepatocytes but maintained in the NPCs with increased abundance (Figure 1B and Figure 1C, red arrow). Using co-immunofluorescence (IF) staining of *Osr1* and F4/80, we found that *Osr1* was expressed in a subset of F4/80+ cells. However, the staining of *Osr1* was not co-labeled with *Clec4e*, the KC-specific marker (Figure 1D). These results suggest that monocyte-derived macrophages are a source of *Osr1*-expressing cells.

Specifically Deleting Osr1 in Myeloid Cells Promoted HFD and MCD-induced Hepatic Steatosis and Inflammation

To identify the cell sources in which *Osr1* contributes to the repression of NAFLD/NASH, we determined whether

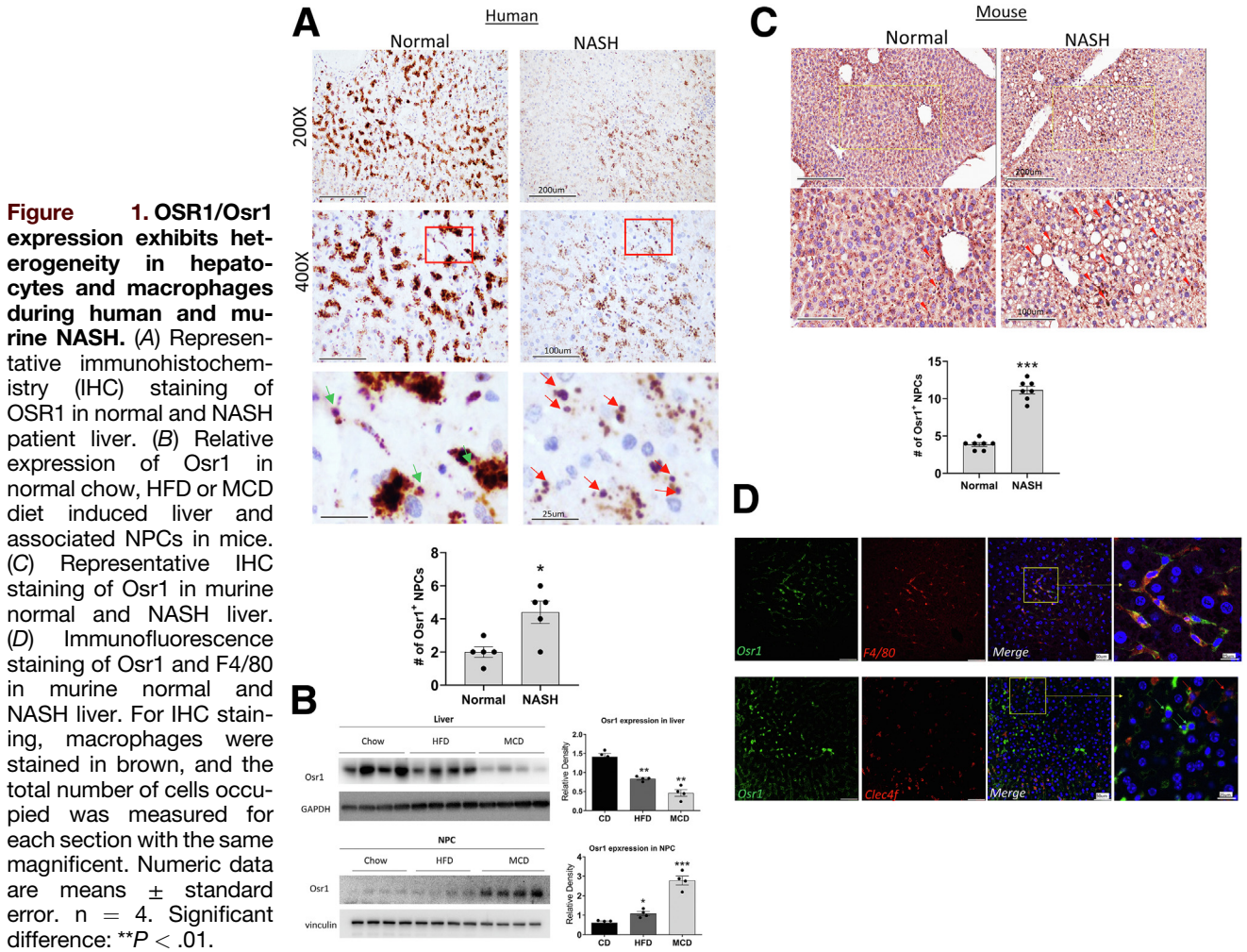
Abbreviations used in this paper: ALT, alanine aminotransferase; AST, aspartate aminotransferase; BMDM, bone marrow-derived macrophage; CD, chow diet; FAO, fatty acid oxidation; FLIM, fluorescence lifetime imaging microscopy; FLIRR, fluorescence lifetime redox ratio; GO, gene ontology; hCLS, hepatic crown-like structures; HFD, high-fat diet; IF, immunofluorescence; IL, interleukin; KC, Kupffer cell; KEGG, Kyoto Encyclopedia of Genes and Genomes; LDL, low-density lipoprotein; LPS, lipopolysaccharide; MCD, methionine- and choline-deficient diet; NAFLD, nonalcoholic fatty liver disease; NAS, NAFLD activity score; NASH, nonalcoholic steatohepatitis; NPC, non-parenchymal cell; OCR, oxygen consumption rate; *Osr1*, odd skipped-related 1; OXPHOS, oxidative phosphorylation; qPCR, quantitative real-time polymerase chain reaction; RNA-seq, RNA sequencing; TG, triglyceride; WD, Western diet.

 Most current article

© 2022 The Authors. Published by Elsevier Inc. on behalf of the AGA Institute. This is an open access article under the CC BY-NC-ND license (<http://creativecommons.org/licenses/by-nc-nd/4.0/>).

2352-345X

<https://doi.org/10.1016/j.jcmgh.2022.12.010>



deleting *Osr1* in hepatocytes or macrophages would promote NAFLD/NASH progression.

Osr1^F, *Osr1^{ΔHep/+}*, and *Osr1^{ΔHep}* mice were fed with either chow diet (CD) or 60% HFD for 12 weeks ($n = 8$). By the end of week 12, the *Osr1^{ΔHep}* mice had a similar weight and liver/body weight ratio to the *Osr1^F* mice, regardless of sex and dietary treatment. All groups had similar intraperitoneal glucose tolerance test results and developed similar levels of steatosis (Figure 2A–D). These results suggest that hepatocyte *Osr1* deletion was not the major contributor to NAFLD progression.

With myeloid-specific *Osr1* deletion, when fed with CD for 20 weeks (Figure 3A), the *Osr1^{ΔMφ}* and control mice had similar body weight, and hepatic steatosis was not developed; however, there was more lipid deposition in the liver of the *Osr1^{ΔMφ}* mice (Figure 3B–C).

Fed with HFD (Figure 3A), significantly higher body weight was observed in the *Osr1^{ΔMφ}* male (Figure 3D) but not female mice (Figure 4A–B), accompanied by worsening glucose intolerance (Figure 3E) and heavier liver (Figure 3F). The *Osr1^{ΔMφ}* male liver exhibited enhanced steatosis with a higher NAFLD activity score (NAS) (Figure 3G), consistent with the higher serum levels of alanine aminotransferase (ALT), aspartate

aminotransferase (AST), and low-density lipoprotein (LDL) (Figure 3H), and the increased hepatic triglyceride (TG) content (Figure 3I). The increased steatosis in the *Osr1^{ΔMφ}* mice was accompanied by the increased expression of lipogenesis genes (Figure 3J). In addition, *Osr1^{ΔMφ}* male liver showed increased macrophage infiltration (Figure 3K), associated with overactivated pro-inflammatory signaling (Figure 3L) and higher pro-inflammatory cytokine mRNA levels (Figure 3M), suggesting more hepatic inflammation in *Osr1^{ΔMφ}* mice.

In the MCD-induced NASH model (Figure 3A), male (Figure 3N) but not female *Osr1^{ΔMφ}* mice (Figure 4C) exhibited more advanced NASH progression, characterized by more macrovesicular steatosis and elevated serum ALT and LDL levels (Figure 3O). Trichrome Masson and Sirius Red staining revealed more collagen deposition in the *Osr1^{ΔMφ}* livers (Figure 3N) with enhanced expression of collagen-producing gene expression (Figure 3P). We observed more inflammation in the *Osr1^{ΔMφ}* livers, characterized by more microgranulomas (Figure 3N, green arrow), F4/80⁺ macrophages, hepatic crown-like structures (hCLS) (Figure 3N, red arrow), and increased expression of pro-inflammatory cytokine genes (*Tnf-α* and *Il-1β*) (Figure 3Q). Western blots demonstrated overactivated pro-

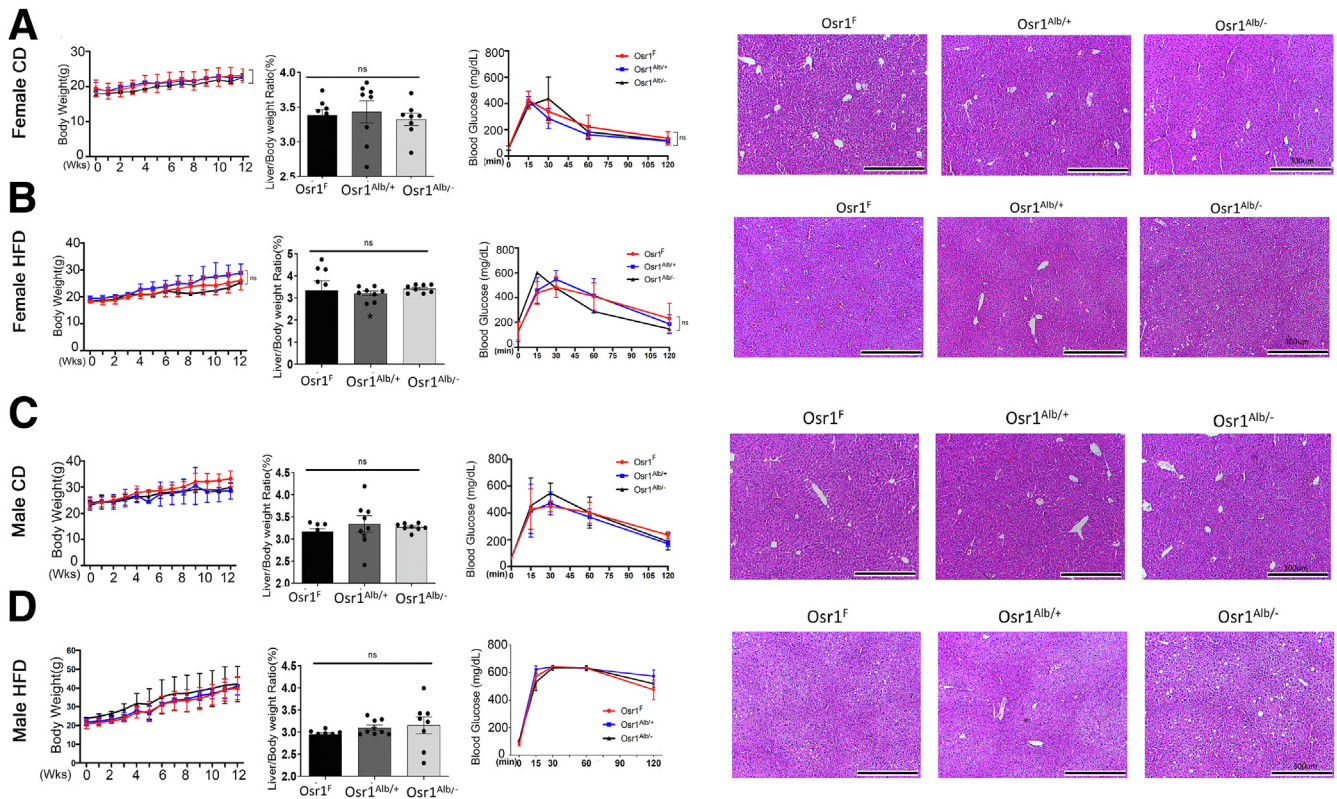


Figure 2. Deleting *Osr1* in hepatocytes did not affect the HFD-induced NAFLD phenotype in either female or male mice.

(A) The body weight change, the liver/body weight ratio, intraperitoneal glucose tolerance test (IPGTT), and representative hematoxylin and eosin (H&E) staining in female *Osr1^F*, *Osr1^{ΔAlb/+}*, and *Osr1^{ΔAlb/-}* mice fed with CD for 12 weeks. (B) The body weight change, the liver/body weight ratio, IPGTT, and representative H&E staining in female *Osr1^F*, *Osr1^{ΔAlb/+}*, and *Osr1^{ΔAlb/-}* mice fed with HFD for 12 weeks. (C) The body weight change, the liver/body weight ratio, IPGTT, and representative H&E staining in male *Osr1^F*, *Osr1^{ΔAlb/+}*, and *Osr1^{ΔAlb/-}* mice fed with CD for 12 weeks. (D) The body weight change, the liver/body weight ratio, IPGTT, and representative H&E staining in male *Osr1^F*, *Osr1^{ΔAlb/+}*, and *Osr1^{ΔAlb/-}* mice fed with HFD for 12 weeks ($n = 8$). Numeric values are presented as means \pm standard error.

inflammatory signaling in the *Osr1^{ΔMφ}* liver (Figure 3Q). To recapitulate human NASH, we further adapted 2 additional NASH models, a relatively rapid STAM model and a chronic Western diet (WD) model, to investigate the role of macrophage *Osr1* in NASH pathogenesis (Figure 3R–S). In both models, myeloid-specific *Osr1* deletion resulted in more severe NASH. The histological investigation revealed more steatosis and ballooning in *Osr1^{ΔMφ}* livers, confirmed by higher total NAS scores (Figure 3R–S). These results suggest that myeloid *Osr1* deletion induces severe NAFLD/NASH progression, with advanced steatosis, fibrosis, and aggravated inflammatory responses in male mice.

Deleting *Osr1* in Myeloid Cells Skewed Macrophage Polarization

To determine how *Osr1* deletion promotes NASH, RNA sequencing (RNA-seq) analysis was performed on the *Osr1^F* and *Osr1^{ΔMφ}* mice fed with CD or MCD (Figure 5A). Gene ontology (GO) analysis identified distinct Kyoto Encyclopedia of Genes and Genomes (KEGG) pathways associated with macrophage plasticity and polarization, including NF- κ B, PPAR, JAK-STAT, and osteoclast differentiation signaling (Figure 5A), suggesting a critical role of *Osr1* in macrophage differentiation and polarization.

To test the hypothesis that *Osr1* regulates macrophage polarization, bone marrow-derived macrophages (BMDMs) were isolated from *Osr1^F* and *Osr1^{ΔMφ}* mice and induced to differentiate in vitro. *Osr1* expression was relatively weak initially (considered M0), and sustained induction of *Osr1* was observed after exposure to interleukin (IL)-4 (Figure 5B). However, the expression pattern of *Osr1* was opposite when exposed to lipopolysaccharide (LPS) (Figure 5B). With *Osr1* deletion, M2-specific genes, including *Arg1*, *Mrc1*, *Ym1*, and *CD36* failed to upregulate upon IL-4 treatment for 24 hours, whereas expression fluctuation was noted on M1-related genes *Cd80*, *Hif1a*, and *Nos2* (Figure 5C). Consistently, *Osr1* deletion resulted in activation of pro-inflammatory p38, JNK, NF- κ B p65 (Figure 5D), and overexpression of pro-inflammatory cytokines genes under basal conditions (M0) or LPS induction (Figure 5D). Similar *Osr1*-associated polarization switches were noted in vivo. MCD-fed mice showed peak inflammatory cytokine production at week 4.¹⁹ A significantly fewer percentage of M2 macrophages was observed in the *Osr1^{ΔMφ}* liver upon 4-week MCD feeding, resulting in a significantly decreased M2/M1 ratio (Figure 5E).

Considering a strong response of *Osr1^{ΔMφ}* BMDMs to LPS, we further explored this phenomenon in vivo. *Osr1^F*

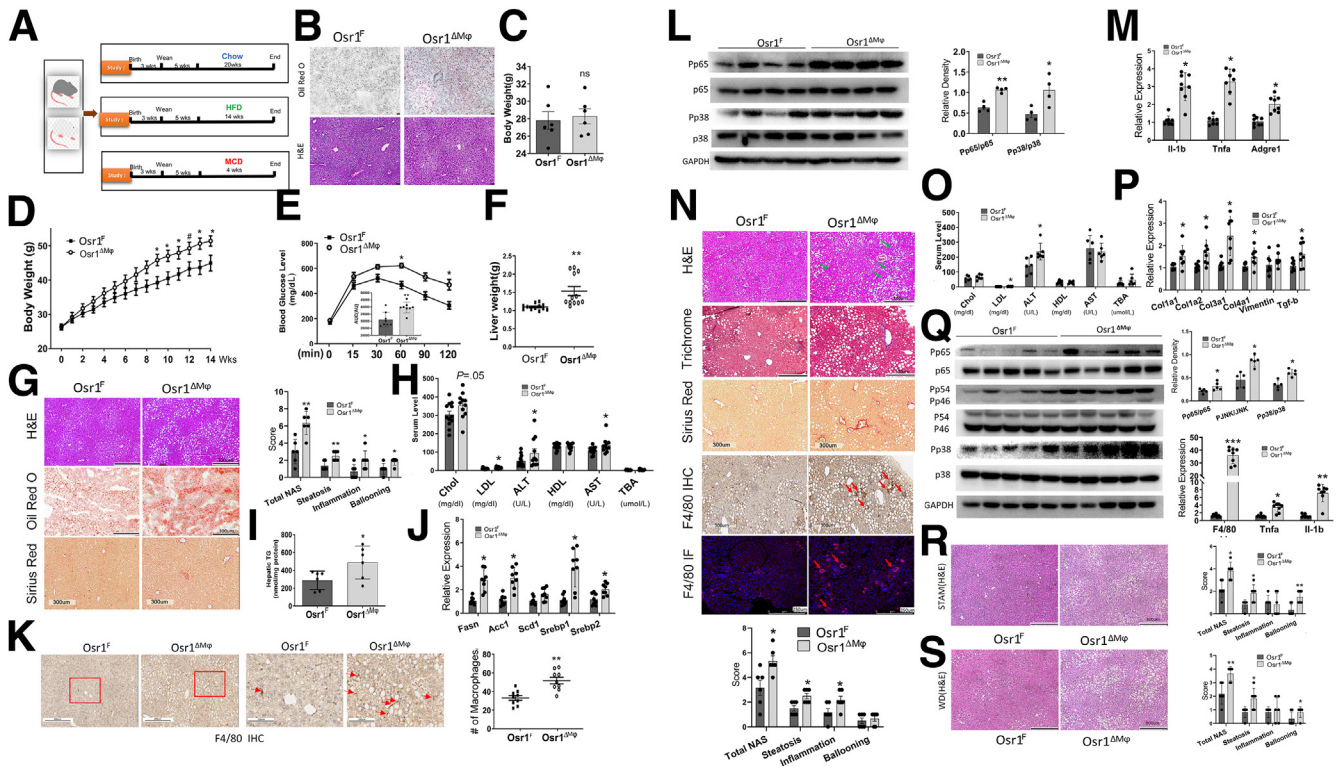


Figure 3. Deletion of macrophage *Osr1* aggravated HFD, and the MCD diet-induced hepatic steatosis and inflammation in mice. (A) *Osr1^F* and *Osr1^{ΔMφ}* mice were treated with CD for 20 weeks, HFD for 14 weeks, or MCD for 4 weeks. (B) Oil red O staining in frozen sections and hematoxylin and eosin (H&E) staining in paraffin embedded sections upon CD. (C) The mean body weight upon CD. (D) Body weight gain upon HFD. (E) Intraperitoneal glucose tolerance test (IPGTT) upon HFD. (F) Liver weight upon HFD. (G) Representative images of H&E, Oil Red-O, or Sirius red staining, and NAS of indicated groups under HFD treatment. (H) Lipid metabolism and liver damage serum markers. (I) Liver triglyceride and de novo lipogenesis-related genes (J) in the liver upon HFD. (K) Quantification of liver macrophages. (L) Liver pro-inflammatory signaling and inflammation-related genes upon HFD (M). (N) Representative images of H&E, Tri-Chrome Masson, Sirius Red, F4/80 immunohistochemistry, and IF staining. NAS of indicated groups under MCD diet treatment. (O) Lipid metabolism and liver damage serum markers. (P) Liver fibrosis-related genes under MCD diet treatment. (Q) Liver pro-inflammatory signaling and genes under MCD diet treatment. (R) Representative images of H&E staining of *Osr1^F* and *Osr1^{ΔMφ}* liver induced with STAM model and associated NAS scoring. (S) Representative images of H&E staining of *Osr1^F* and *Osr1^{ΔMφ}* liver under WD treatment for 20 weeks and associated NAS scoring. For (K) and (N) macrophages were stained in brown, and the total area occupied by these cells was measured. Numeric data are means ± standard error. n = 8–12. Significant differences between *Osr1^F* and *Osr1^{ΔMφ}* are indicated as follows: **P* < .05; ***P* < .01; ****P* < .001.

and *Osr1^{ΔMφ}* mice were exposed to HFD for 12 weeks and were intraperitoneally injected with LPS (100 ug/kg/day) for the last 4 weeks of HFD treatment. Liver histology indicated that *Osr1^{ΔMφ}* mice exhibited more advanced NASH progression with increased inflammation levels (Figure 5F), which is consistent with our in vitro study.

PPARγ and *c-Myc* are Direct Targets of *Osr1* for Regulating Macrophage Alternative M2 Polarization

Our RNA-seq analysis identified differential expression of *c-Myc* and *Pparγ* in the *Osr1^{ΔMφ}* vs *Osr1^F* liver under both CD and MCD. Confirmed in the BMDMs, *PPARγ* and *c-Myc* expression were associated with *Osr1* level during the phenotype switch between M1 and M2 (Figure 6A). However, *PPARγ* and *c-Myc* expression no longer responded to IL-4 induction upon *Osr1* deletion (Figure 6B). *Osr1*

overexpression in RAW264.7 cells resulted in increased expression of *PPARγ* and *c-Myc* (Figure 6C). These results suggest that *PPARγ* and *c-Myc* expression depends on *Osr1*.

To determine whether *Osr1* regulates the transactivation of *PPARγ* and *c-Myc*, we performed a bioinformatically incorporative analysis. We identified potential genomic regions of *c-Myc* and *PPARγ* that were further determined by chromatin immunoprecipitation quantitative real-time polymerase chain reaction (qPCR) (Figure 6D) and luciferase reporter assay (Figure 6E). To establish the functional *Osr1*-*PPARγ* regulation in macrophage polarization, *Osr1^F* or *Osr1^{ΔMφ}* BMDMs were treated with IL-4 in the presence of rosiglitazone, a *PPARγ* agonist. Although rosiglitazone failed to fully rescue the expression of *Mrc1* and *c-Myc* in *Osr1^{ΔMφ}* BMDMs, it rescued the typical response to IL-4, a signature of enhanced expression of *Arg1*, *Ym1*, and *CD36* (Figure 6F). Simultaneously, the expression level of the 4 M1 markers except for *Hif1a* were similar in *Osr1^F* and *Osr1^{ΔMφ}* BMDMs

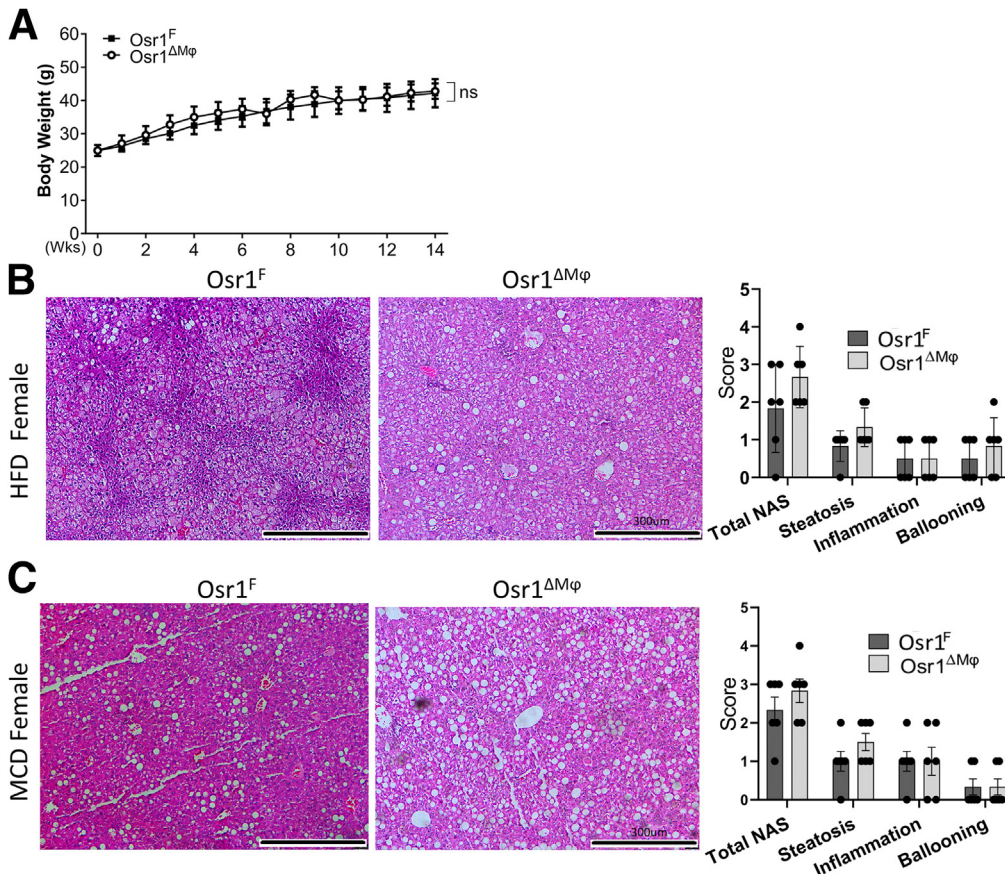


Figure 4. Deleting macrophage *Osr1* did not affect the experimental NASH phenotype in female mice. (A) The mean body weight in female *Osr1^F* and *Osr1^{ΔMφ}* mice fed with HFD for 12 weeks. (B) Representative images of hematoxylin and eosin (H&E) staining and NAS score for liver sections from female *Osr1^F* and *Osr1^{ΔMφ}* mice under HFD treatment. (C) Representative images of H&E staining and NAS score for liver sections from female *Osr1^F* and *Osr1^{ΔMφ}* mice under MCD diet treatment for 4 weeks. Numeric data is presented as means ± standard error.

(Figure 6F). These findings suggest that *PPARγ* and *c-Myc* are downstream targets of *Osr1* in macrophage polarization.

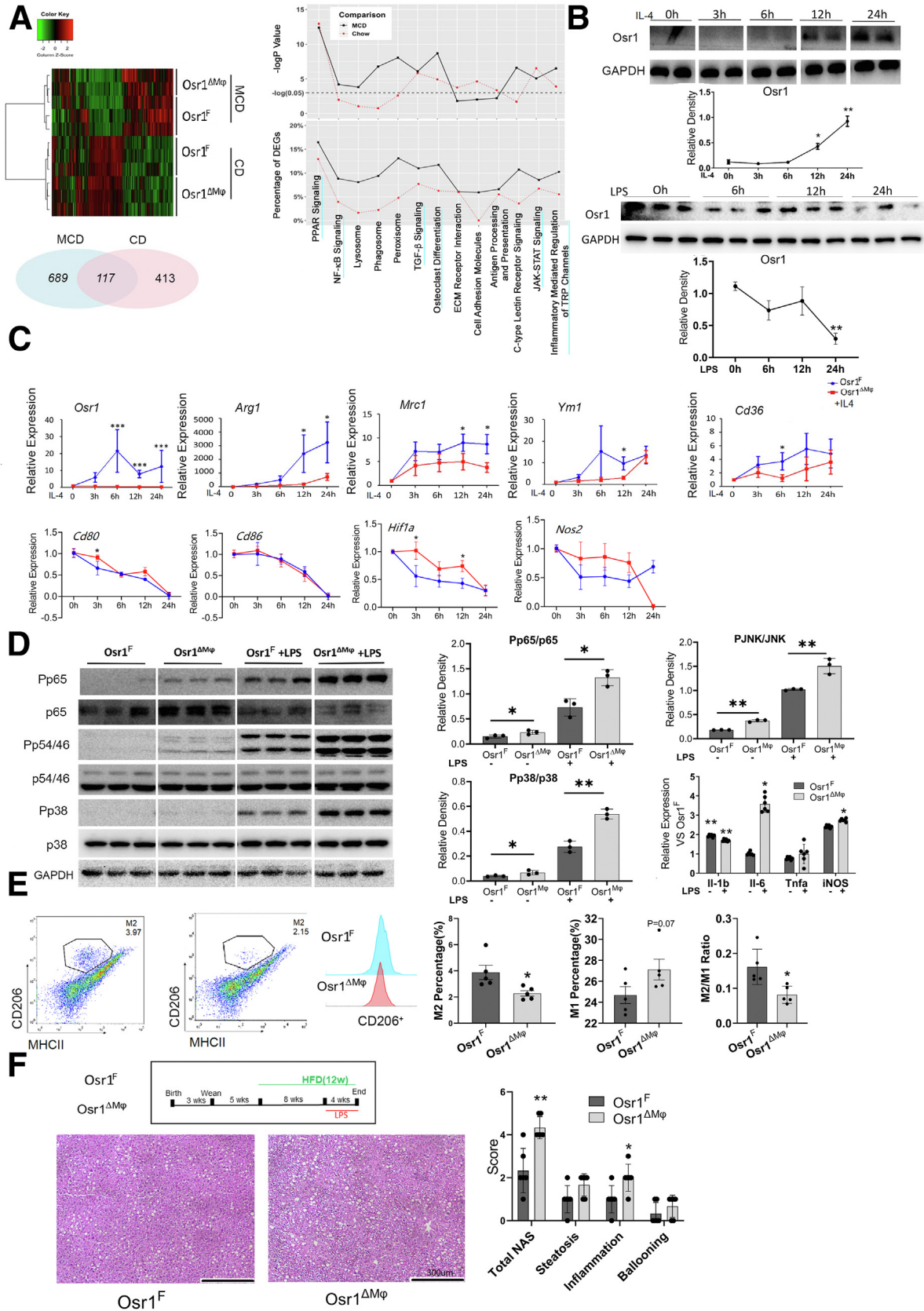
Osr1 is Required for Palmitate Oxidation, and Deleting *Osr1* Shifted Macrophage Metabolism Toward a Glycolysis-dependent ATP Production Profile

Cellular metabolism reprogramming is a hallmark of macrophage polarization. With glucose and pyruvate as substrates, the total ATP production rates were similar in *Osr1^F* and *Osr1^{ΔMφ}* macrophages; however, deleting *Osr1* caused a 25% reduction in the OXPHOS rate (Figure 7A) ($66.53\% \pm 1.43\%$ vs $59.38\% \pm 2.55\%$; $P < .001$) and a 21.4% increase in the glycolysis rate (Figure 7A) ($33.47\% \pm 1.43\%$ vs $40.6\% \pm 2.55\%$; $P < .001$), resulting in an increased ratio in glycolysis vs OXPHOS (Figure 7A). Similarly, deleting *Osr1* significantly reduced the OXPHOS rate (Figure 7B) and increased the rate of glycolysis during M2 induction (Figure 7B). With the presence of rosiglitazone, the skewed glycolysis and OXPHOS in *Osr1^{ΔMφ}* BMDMs were recovered (Figure 7B). Deleting *Osr1* led to an impaired response to PA, evidenced by about 30% lower basal and maximal oxygen consumption rate (OCR), which were recovered by rosiglitazone (Figure 7C). These findings suggest that *Osr1* helps maintain FAO, which depends on *PPARγ*.

The OXPHOS activity consumes NADH (increased NADH-enzyme-bound fraction) and produces FAD (decreased FAD-enzyme-bound fraction).²⁰ To determine whether *Osr1* targets mitochondrial OXPHOS, we applied fluorescence lifetime imaging microscopy (FLIM) to track the mitochondrial NAD(P)H and FAD at the single-cell level (Figure 7D). *Osr1* deletion resulted in a decreased enzyme-bound NAD(P)H intensity in the M2 but not M0 and M1 BMDMs (Figure 7D). From the mitochondrial fluorescence lifetime redox ratio (FLIRR), defined as the fraction of bound NAD(P)H (α_2) divided by the fraction of bound FAD (α_1),²⁰ we observed significantly decreased FLIRR in the *Osr1^{ΔMφ}* M2 but not the M0 and M1 (Figure 7D). These results suggest an impaired mitochondrial OXPHOS in the *Osr1^{ΔMφ}* M2 BMDMs. When PA was given to M2 macrophages, *Osr1^{ΔMφ}* M2 BMDMs exhibited decreased enzyme-bound NAD(P)H intensity and FLIRR, entirely recovered by rosiglitazone treatment (Figure 7D). A lower FLIRR value was also found in the *Osr1^{ΔMφ}* M0 BMDMs under PA treatment. These findings suggest that deleting *Osr1* significantly disrupts OXPHOS in M2 BMDMs.

Deleting Macrophage *Osr1* Aggravated the Inflammation and Fat Deposition in Hepatocytes via Cytokine Production

To determine how inflamed *Osr1^{ΔMφ}* macrophages disrupt lipid homeostasis and promote inflammation in



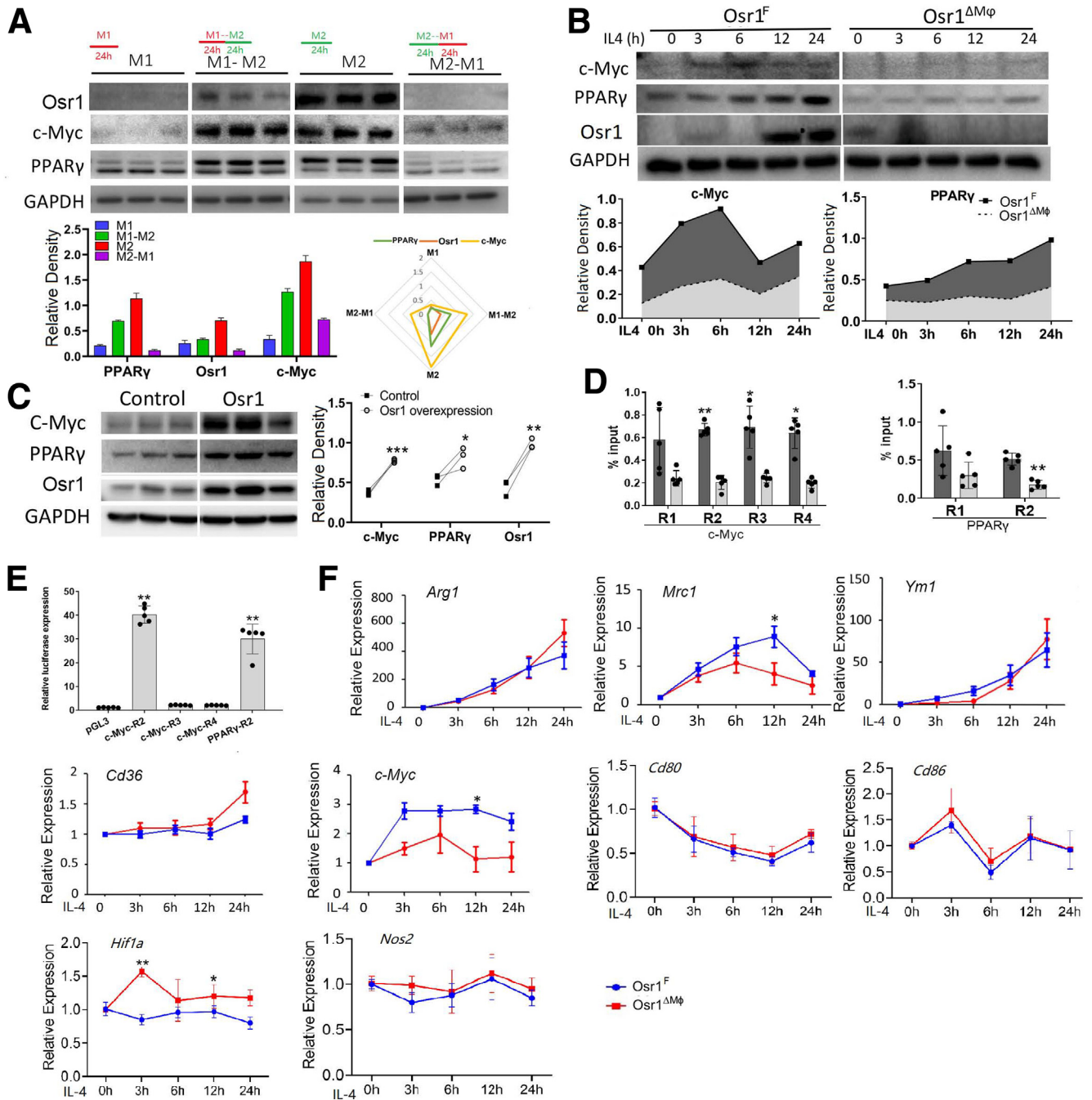


Figure 6. *Osr1* directly transactivated *PPAR-γ* and *c-Myc* in macrophages. (A) The expression level of *Osr1*, *PPARγ*, and *c-MYC* upon M1 induction, M2 induction, M1-M2 switch (M1 switch to M2 induction), and M2-M1 switch (M2 switch to M1 induction). (B) Expression of the *PPARγ* and *c-MYC* in M0 and after exposure to IL-4 in *Osr1^F* and *Osr1^{ΔMφ}* BMDMs. (C) *PPARγ* and *c-MYC* expression in indicated RAW264.7 cells. (D) Chromatin immunoprecipitation-qPCR of *Osr1* in *c-MYC* and *PPARγ* promoters. (E) Relative luciferase activities compared with control. (F) M2 or M1 marker mRNA levels relative to M0 in 1 μ M rosiglitazone. BMDMs were obtained from bone marrow and induced to M0 macrophages with 50 ng/mL M-CSF. The induced macrophages were further stimulated with lipopolysaccharide (LPS, 0.1 μ g/mL) and interferon- γ (IFN- γ , 20 ng/mL) or with IL-4 (20 ng/mL) to induce polarization toward M1 or M2 phenotypes, respectively. Results are displayed as means \pm standard error. * $P < .05$; ** $P < .01$; *** $P < .001$.

Figure 5. (See previous page). *Osr1* was required for macrophage alternative M2 polarization in vivo and in vitro. (A) Heat map and pie chart indicated differentially expressed genes (DEGs). The GO analysis and distinct KEGG pathways associated with *Osr1* level on CD or MCD. Upper panel, any $-\log P$ value higher than the dotted line was identified as significant ($P < .05$). Lower panel, the y-axis indicates the percentage of DEGs. (B) Relative expression of *Osr1* in resting macrophages (M0) and after exposure to IL-4 or LPS. (C) Expression of M1 and M2 markers relative to M0 after resting to IL-4 in the presence or absence of *Osr1*. (D) Pro-inflammatory signaling and cytokine production. (E) Quantification for M1 and M2 macrophages. (F) Representative hematoxylin and eosin staining and the associated NAS for *Osr1^F* and *Osr1^{ΔMφ}* mice liver when exposed to LPS under 12 weeks of HFD treatment (n = 6). Results were shown as means \pm standard error of n = 8 independent experiments. * $P < .05$; ** $P < .01$; *** $P < .001$.

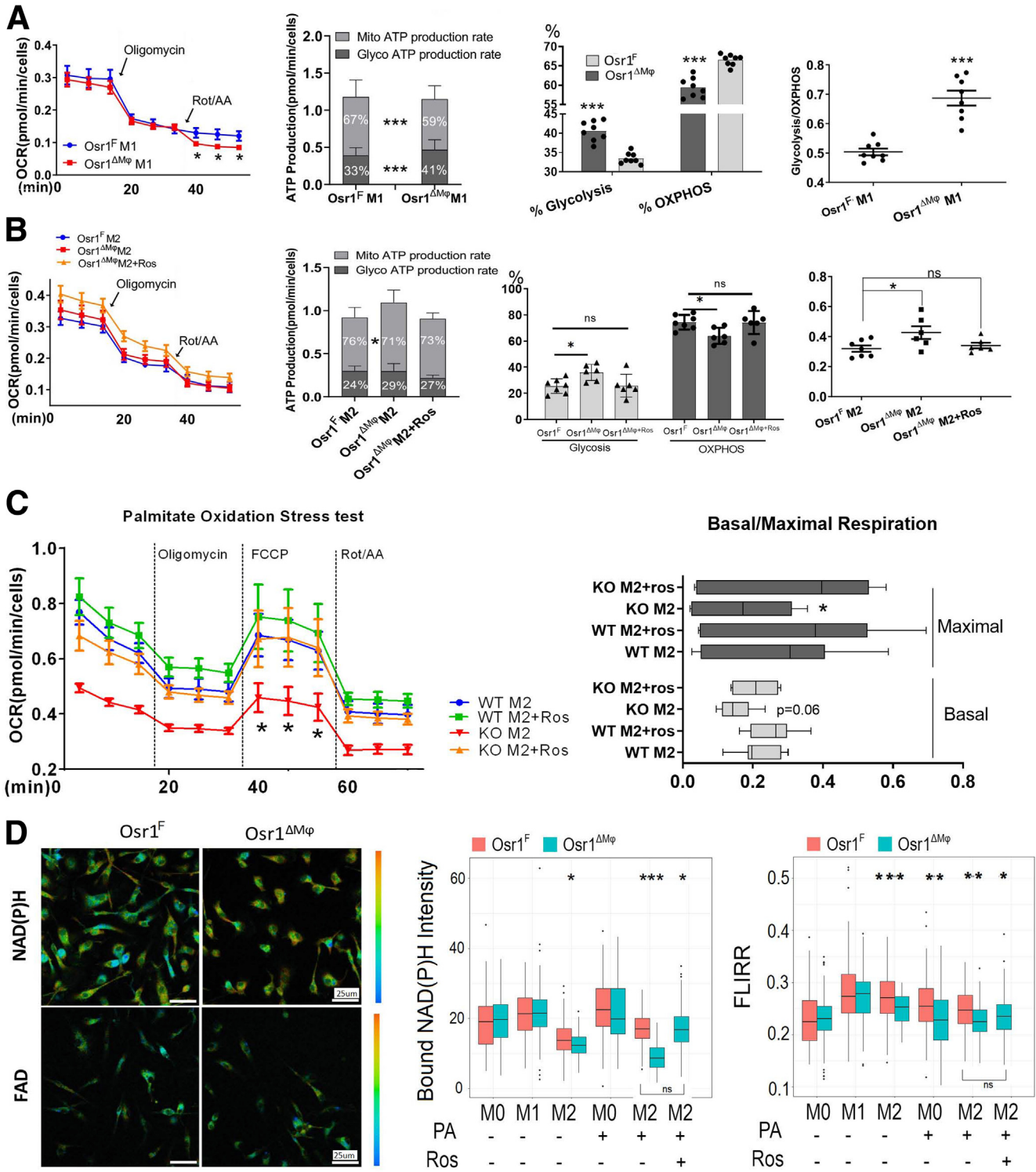


Figure 7. *Osr1* deletion shifted the macrophage to glycolysis ATP production profile and disrupted the mitochondrial palmitate oxidation during M2 polarization. (A–B) Real-time APT rate analysis in *Osr1^F* or *Osr1^{ΔMφ}* BMDMs during M1 (A) or M2 (B) polarization. (C) Mitochondrial respiration function assessed by Seahorse Mito Stress test using palmitate (BSA-conjugated palmitate) as substrates. OXPHOS parameters were assessed by recording the OCR values after sequential OM, FCCP, and Rot+AA injection. (D) Representative images of converted NAD(P)H and FAD under FLIM. The calculated intensity of the bounded form of NAD(P)H and mitochondrial FLIRR was plotted with indicated induction in bar graphs (right 2 panels). AA, Antimycin A; FCCP, carbonyl cyanide-4 (trifluoromethoxy) phenylhydrazone; OM, oligomycin; Ros, rosiglitazone; Rot, rotenone. The number of cells analyzed for FLIM: 62, 75, 240, 154, 133 for M0, M0+PA, M1, M2, M2+PA, respectively, in *Osr1^F* group, and 102, 79, 112, 39, 65, 254 for M0, M0+PA, M1, M2, M2+PA, M2+PA+Ros, respectively, in *Osr1^{ΔMφ}* BMDMs. The analysis is completed using R programming. **P* < .05; ***P* < .01; ****P* < .001.

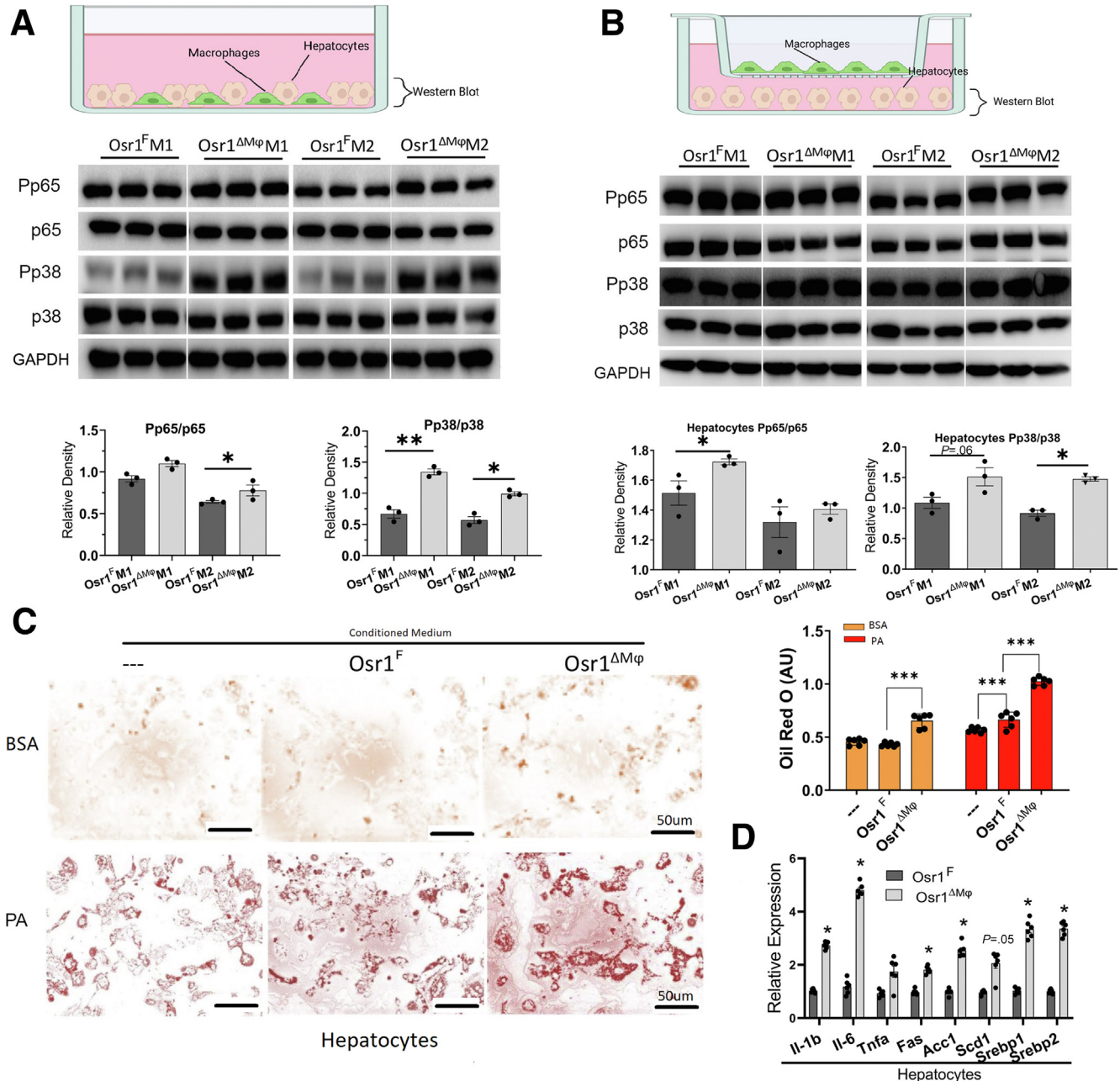


Figure 8. *Osr1* disruption in macrophages aggravated hepatocyte inflammation and fat deposition via cytokine excretion. (A) Pro-inflammatory signaling in macrophage-hepatocyte co-cultured cell lysates. (B) Pro-inflammatory signaling in hepatocytes transwell co-cultured with macrophages. (C) Representative hepatocyte fat deposition in conditioned medium from *Osr1^F* and *Osr1^{ΔMφ}* macrophages. (D) The mRNA levels of lipogenesis and pro-inflammatory cytokines from hepatocytes cultured in the conditioned medium. Numeric data are presented as means \pm standard error ($n = 6$). Significant differences are indicated as follows: * $P < .05$; ** $P < .01$; *** $P < .001$.

hepatocytes, 3 sets of macrophages and hepatocytes co-culture were conducted. First, when primary hepatocytes were co-cultured with the *Osr1^{ΔMφ}* M2 BMDMs, the cell mixture had significantly higher Pp65/p65 and Pp38/p38 ratios than the cell mixture co-cultured with the *Osr1^F* M2 BMDMs (Figure 8A). Similarly, the cell co-culture of *Osr1^{ΔMφ}* M1 BMDMs and hepatocytes displayed overactivation of p38 signaling, supported by an increased Pp38/p38 ratio (Figure 8A). Second, using a transwell system, we observed

higher ratios of Pp65/p65 ($P < .05$) and Pp38/p38 ($P = .06$) in the hepatocytes co-cultured with M1 *Osr1^{ΔMφ}* BMDM than those with *Osr1^F* M1 BMDMs (Figure 8B). The hepatocytes co-cultured with M2 *Osr1^{ΔMφ}* BMDMs significantly increased the Pp38/p38 ratio (Figure 8B). Third, hepatocytes cultured with *Osr1^{ΔMφ}*-conditioned medium significantly increased lipid deposition under BSA and PA treatment (Figure 8C) associated with elevated mRNA levels of pro-inflammatory cytokines (*Tnfa*, *Il-6*, and *Il-1 β*) and de novo lipogenesis

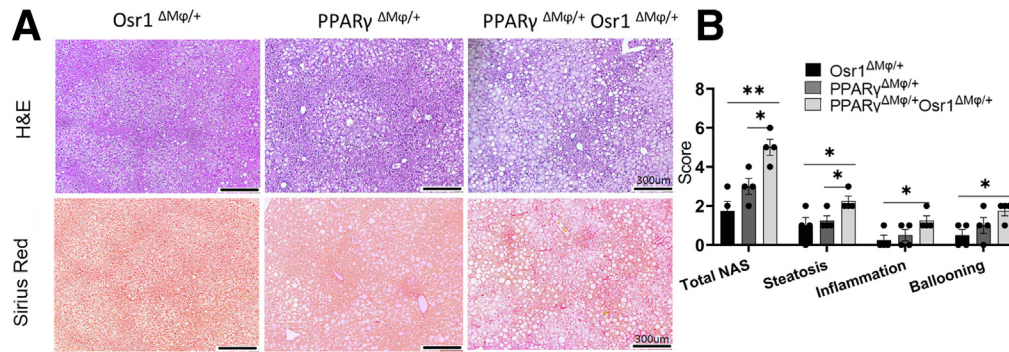


Figure 9. *Osr1* and *PPARγ* functionally interacted in macrophages during the pathogenesis of NAFLD/NASH. (A) Hematoxylin and eosin and Sirius red staining in the indicated mice. (B) NAS scoring in the indicated mice during HFD treatment for 12 weeks. Numeric data are presented as means \pm standard error. Significant differences are indicated as follows: * $P < .05$, ** $P < .01$.

genes (Figure 8D). These findings suggest that deleting macrophage *Osr1* aggravates hepatocyte inflammation and fat deposition by modulating cytokine production.

Pharmacological Activation of *PPARγ* Signaling Prevented HFD-induced Steatohepatitis in *Osr1*^{ΔMφ} Mice

To determine the functional role of *Osr1*-*PPARγ* regulation in NASH progression, we performed genetic and in vivo pharmacological studies using rosiglitazone. In the genetic study, compound heterozygotes of *Osr1* and *PPARγ* (*Osr1*^{ΔMφ/+}*PPARγ*^{ΔMφ/+}) and their littermate control mice were induced to develop NAFLD. The NAFLD progression of the *Osr1*^{ΔMφ/+} and the *PPARγ*^{ΔMφ/+} livers were similar. However, the *Osr1*^{ΔMφ/+}*PPARγ*^{ΔMφ/+} livers displayed more advanced NASH with higher NAS, with higher scores in steatosis, inflammation, and hepatocyte ballooning than their littermate controls (Figure 9A–B).

Rosiglitazone treatment significantly reduced the body weight gain (Figure 10A–B) and improved glucose intolerance at week 14 in *Osr1*^{ΔMφ} mice (Figure 10C), whereas the liver weight or liver/body weight ratio remained the same (Figure 10D). Further analysis in liver lysates indicated more sensitized insulin signaling in rosiglitazone-treated *Osr1*^{ΔMφ} mice (Figure 10E).

Significantly lower serum ALT and LDL levels (Figure 10F), improved NAFLD phenotype (Figure 10G), and reduced TG content in perfused hepatocytes and liver (Figure 10H) were observed in the *Osr1*^{ΔMφ} mice treated with rosiglitazone. The *Osr1*^{ΔMφ} mice livers revealed lower numbers of infiltrated macrophages (Figure 10I) and deactivated pro-inflammatory signaling (Figure 10J) under rosiglitazone treatment. A treatment effect of rosiglitazone was also noticed in the *Osr1*^F liver as indicated by a lower NAS score, less steatosis and ballooning hepatocytes (Figure 10G).

Inducing *Osr1* Expression Therapeutically Improved the NAFLD/NASH of the *Osr1*^{ΔMφ} Mice

In mouse models, we assessed the feasibility of targeting *Osr1* for NAFLD/NASH treatment (Figure 11A). AAV8L

transduction efficiency was confirmed by fluorescence-activated cell sorting showing that about 17% of the F4/80⁺ population was infected by AAV8L after AAV8L-GFP injection for 4 weeks (Figure 11B) and before the special diet treatment. After HFD treatment for 14 weeks, wild-type mice injected with AAV8L-*Osr1* had about a 40% increase in *Osr1* expression in hepatic NPCs by comparing with the control group (Figure 11C). The NPC expression of *PPARγ* was also increased upon AAV8L-*Osr1* transduction (Figure 11C). The co-IF staining further indicated that the AAV8L-*Osr1* efficiently replenished the *Osr1* expression in *Osr1*^{ΔMφ} mice macrophages (Figure 11D, yellow arrow).

When fed with HFD, the body weights of *Osr1*^{ΔMφ} mice with AAVL-*Osr1* were significantly lower than those with AAVL-control treatment. Similarly, the *Osr1*^F mice with AAVL-*Osr1* had marginally lower body weights than those with AAVL-control (Figure 11E). AAV8L-*Osr1* administration reversed the glucose intolerance in *Osr1*^{ΔMφ} mice during HFD treatment compared with *Osr1*^F mice (Figure 11F). The *Osr1*^{ΔMφ} mice with AAVL-*Osr1* presented similar liver weight with that of AAV8L-*Osr1*^F mice (Figure 11G). Regarding liver histology, *Osr1* replenishment improved liver steatosis and inflammation in the *Osr1*^{ΔMφ} mice (Figure 11H). *Osr1* replenishment rescued liver inflammation in the *Osr1*^{ΔMφ} mice by reduced macrophage infiltration (Figure 11I) with recovered M2 sub-populations and M2/M1 ratios. Interestingly, *Osr1* overexpression also improved the NASH score, enlarged the M2 macrophage sub-population, and increased the M2/M1 ratio in *Osr1*^F mice (Figure 11J). We also observed reduced proinflammatory cytokine mRNA levels during AAV8L-*Osr1* administration (Figure 11K). These findings suggest that rescuing *Osr1* expression improves NAFLD/NASH and liver inflammation.

Discussion

We established the role of *Osr1* in macrophage metabolism and polarization and elucidated its associated functions in the inflammation-induced pathogenesis of NASH (Figure 12). Using mouse models with myeloid *Osr1* deletion, we observed aggravated NAFLD/NASH progression induced by HFD or MCD, suggesting the protective role of

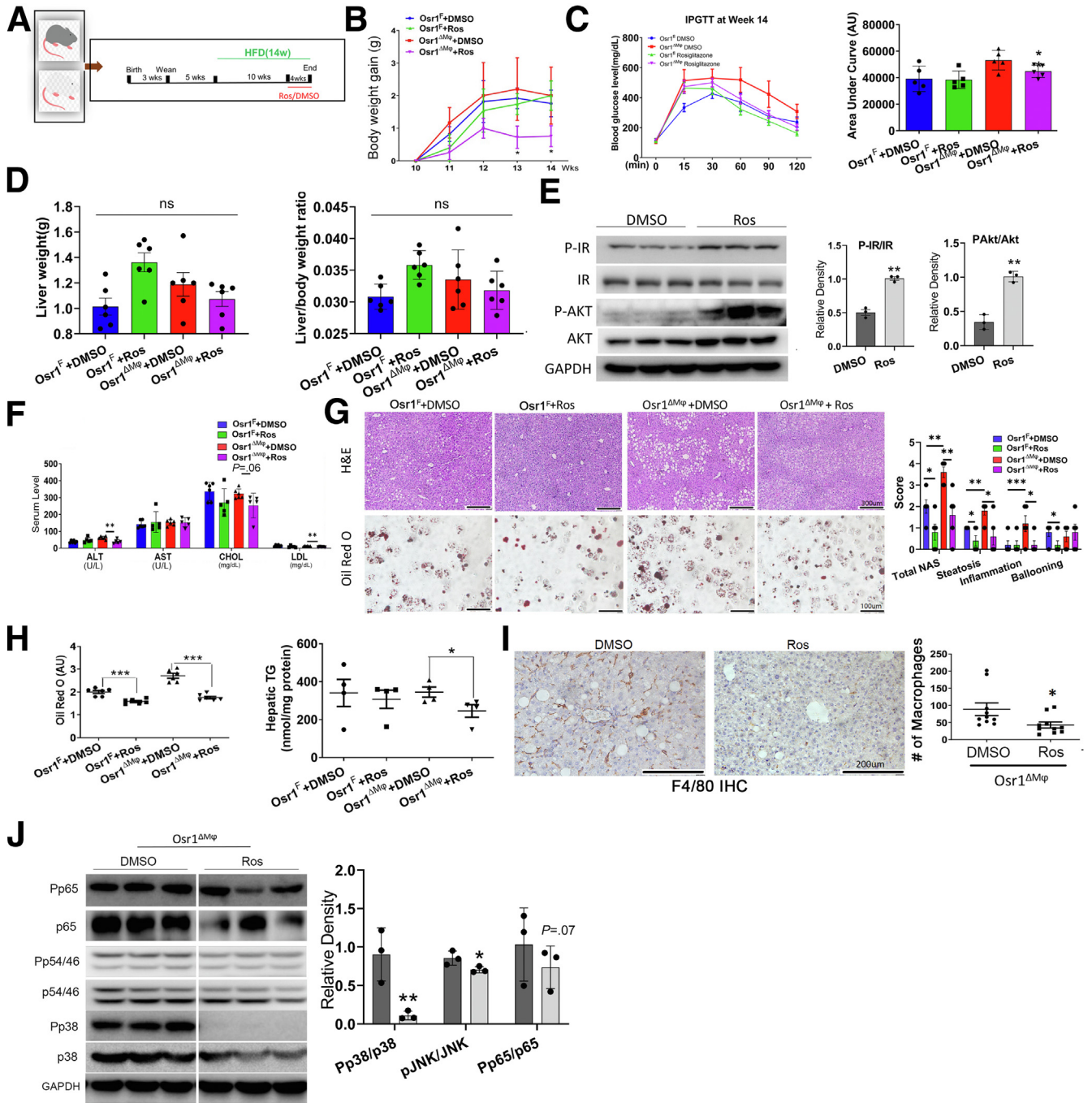
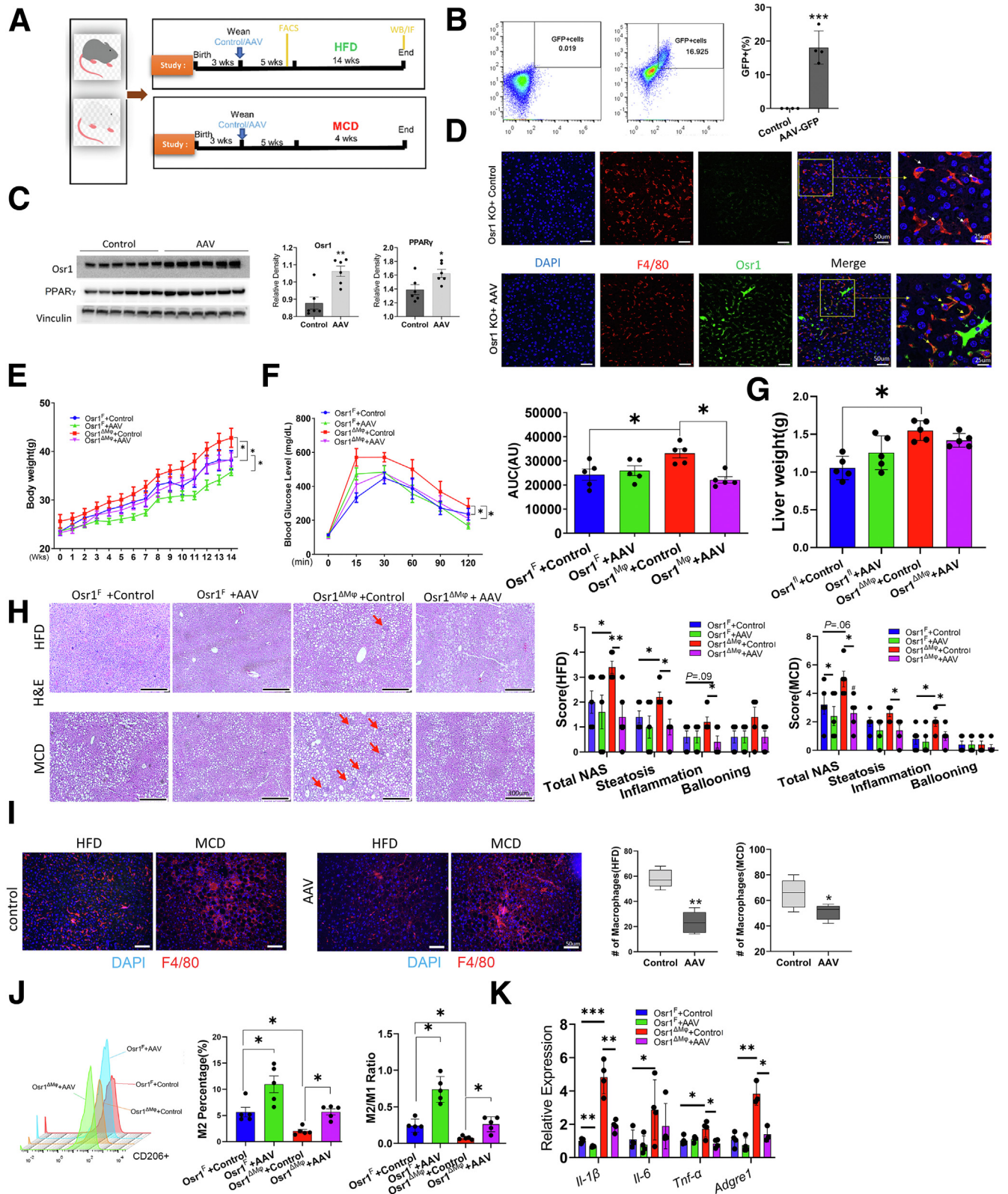


Figure 10. Pharmacological PPAR γ agonist rosiglitazone prevented HFD induced liver injury and inflammation in *Osr1^{ΔMφ}* mice. (A) Schematic diagram for the study design with HFD and rosiglitazone. DMSO or rosiglitazone was administered to *Osr1^F* and *Osr1^{ΔMφ}* mice at 10 mg/kg/day during the final 4 weeks of the total 14 weeks of HFD treatment. (B) Body weight gain during the rosiglitazone/DMSO treatment. (C) Intraperitoneal glucose tolerance test (IPGTT) results and the area under the curve (AUC) in indicated groups after the rosiglitazone treatment. (D) Liver weight and liver/body weight ratio in indicated mice. (E) Prior to harvest, mice were intraperitoneally injected with insulin or DMSO. Insulin signaling of the extracted proteins from the *Osr1^{ΔMφ}* liver were inspected. (F) Lipid metabolism and liver damage serum markers. (G) NAS score, representative hematoxylin and eosin (H&E) staining, Oil Red O staining in perfused hepatocytes and associated quantification, and TG level in the liver (H). (I) Quantification of macrophage numbers in *Osr1^{ΔMφ}* liver. (J) Pro-inflammatory signals in *Osr1^{ΔMφ}* liver. For F4/80 immunohistochemical (IHC) staining, macrophages were stained brown, and the total number of cells occupied was measured for each section with the same magnification. Numeric data are presented as means \pm standard error (n = 6–8). Significant differences are indicated as follows: * $P < .05$; ** $P < .01$; and *** $P < .001$. DMSO, Dimethyl sulfoxide; Ros, rosiglitazone.

macrophage *Osr1* in NAFLD/NASH pathogenesis. Deleting *Osr1* in macrophages resulted in the glycolysis-dependent energy metabolism and a polarization switch toward an

inflammatory M1 phenotype. We identified *c-Myc* and *PPAR γ* as the direct downstream targets of *Osr1* in macrophage polarization. With a genetic study using myeloid-



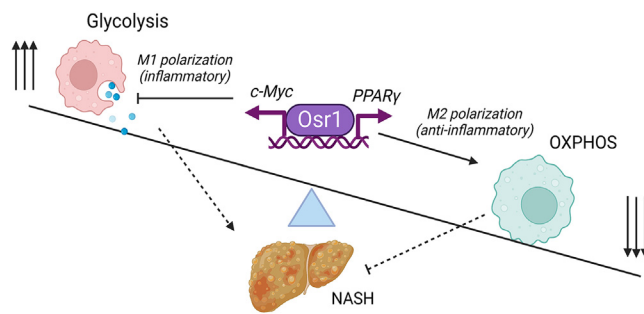


Figure 12. *Osr1* regulates macrophage-mediated liver inflammation in non-alcoholic fatty liver disease progression. Schematic diagram of the mechanisms of NASH induced in *Osr1*^{ΔMφ} mice. The *Osr1*-PPAR γ cascade is a potential driver for macrophage M2 polarization by regulating cellular OXPHOS. Deleting *Osr1* induced metabolic imbalance of glycolysis/OXPHOS in macrophages, promoting pro-inflammatory responses and steatosis in the liver.

specific *Osr1* and PPAR γ compound heterozygote mice and a pharmaceutical PPAR γ activation study, we elucidate a functional macrophage *Osr1*-PPAR γ transcriptional cascade in liver inflammation and the associated NAFLD/NASH. Most importantly, by improving liver inflammation and recovering the macrophage M2/M1 ratio, AAV8L-*Osr1* replenishment/overexpression inhibited liver inflammation, contributing to improved NASH.

Osr1 has been widely studied for embryonic development^{12,13,21} and tumorigenesis.^{14,15,22} However, its role in metabolism and inflammation has never been reported, even though it has been decades since the *Odd*, *Osr1* homolog in *Drosophila* was found to mark plasmatocyte (*Drosophila* macrophage).²³ In HFD/MCD diet-induced NAFLD/NASH models, myeloid-specific *Osr1* deletion resulted in decreased M2 percentiles and M2/M1 ratios associated with elevated pro-inflammatory responses in the liver. These results suggest that *Osr1* regulates macrophage polarization, probably by maintaining the M2 phenotype. Our study provides solid evidence to support this finding. First, *Osr1* expression increased during macrophage M2 commitment, with decreased expression when switching to M1. Second, the *Osr1* expression level correlated with M2 markers during downregulation or overexpression. Finally, *Osr1*-responsive genomic regions of PPAR γ and *c-Myc* were identified. PPAR γ plays a pivotal role in promoting the M2 phenotype switch by upregulating CD206 and CD163²⁴ and modulating Kupffer M1/M2 polarization.²⁵ Similarly, *c-Myc*

resolved inflammation and drove macrophage M2 polarization.²⁶ In our study, rosiglitazone rescued M2 polarization both in vitro and in vivo, demonstrating the functional role of the *Osr1*-PPAR γ axis in this process. Thus, we identified a novel hierarchical network led by *Osr1* (involving PPAR γ and *c-Myc*) in modulating macrophage plasticity toward M2.

Macrophage infiltration of both M1 and M2 types is a signature of liver inflammation. *Osr1* expression was found in a subpopulation of, but not all F4/80+ cells in the MCD-induced NASH model. In vitro, strong *Osr1* expression was observed in the M2 and the transitional type (M1-M2) of macrophages. These data suggested that *Osr1*+ macrophages might be characterized by an intrinsic ability to switch plasticity during the progression of liver inflammation. Unfortunately, our data did not further address the exact phenotype of *Osr1*+ macrophages in the MCD-induced NASH model. However, we excluded that *Osr1*+ macrophages were a source of or derived from KCs, because *Osr1* did not co-express with the KC marker, *Clec4f*. Future studies will need to further characterize the plasticity of *Osr1*-expressing macrophages under both physiological and pathophysiological status.

Macrophage polarization is accompanied by metabolic reprogramming, switching from an OXPHOS-based aerobic profile to a glycolysis-based anaerobic one and vice versa.²⁷ Alternative macrophage polarization relies on the transcription factor PPAR γ , its coactivator PGC1 β , and its downstream target CD36,²⁸ which promote FAO and mitochondrial OXPHOS. A potential role of *Osr1* in metabolic reprogramming was highlighted by identifying its role in transactivating PPAR γ . In our study, deleting *Osr1* resulted in an increased ratio of glycolysis to OXPHOS in M1 and M2 BMDMs. During M2 polarization, deleting *Osr1* significantly blocked OXPHOS, suggesting that *Osr1* maintains OXPHOS in M2 BMDMs. Metabolic changes were pronounced under PA treatment. PA is elevated in NAFLD patients' blood and induces metabolic inflammation by activating NF- κ B signaling in metabolically-activated macrophages.^{29,30} In contrast, PA activates the anti-inflammatory PPAR γ by unknown mechanisms.^{24,30} In our study, deleting *Osr1* blocked the PA oxidation and the anti-inflammatory effects of PPAR γ , supporting the notion that the anti-inflammatory effect in macrophages is mediated by *Osr1*. Our FLIM data did not determine whether *Osr1* regulates glycolysis because FLIM does not resolve cytoplasmic enzyme-bound NAD(P). *Osr1* may inhibit the inflammatory response of M1 BMDMs via *c-Myc* signaling, considering the negative role of *c-Myc* in

Figure 11. (See previous page). AAV8L-delivered *Osr1* expression rescued NAFLD/NASH of the *Osr1*^{ΔMφ} mice. (A) Schematic diagram for the study design with special diet treatment and AAV infection. Mice were injected with pAAV8L-control or pAAV8L-*Osr1* at the dosage of 1.0×10^{10} gc/mouse at wean (3 weeks of age) through retro-orbital venous sinus delivery, followed by HFD or MCD treatment for either 14 or 4 weeks. The time point when the fluorescence-activated cell sorting (B), Western blot (C), and IF staining (D) were conducted were indicated. (E) Body weight at sacrifice. Mice were fed with HFD for 14 weeks. (F) Intraperitoneal glucose tolerance test (IPGTT) results at 12 weeks of HFD and associated quantification. (G) Liver weight upon HFD treatment. (H) Representative hematoxylin and eosin (H&E) staining and NAS scoring under HFD and MCD treatment. (I) Representative IF staining of F4/80 and quantification. (J) Macrophage polarization in the liver. (K) Pro-inflammatory cytokines mRNA level. M1 and M2 macrophages were identified as CD45⁺F4/80⁺CD11b⁺MHCII⁺ CD206⁻ and CD45⁺F4/80⁺CD11b⁺CD206⁺MHCII⁻, respectively. Results are presented as means \pm standard error of n = 5 independent experiments. Significant differences are indicated as follows: **P* < .05; ***P* < .01.

macrophage glycolysis during the early stage of M1 polarization.³¹ Further information, such as *Osr1*-associated lactate production, needs to be elucidated.

Our attempts to interfere with NASH/NAFLD progression by targeting *Osr1*-mediated macrophage inflammation are promising. Mice with AAV8L-delivered *Osr1* expression reduced liver inflammation with less macrophage infiltration and corrected M2/M1 ratios, significantly improving NAFLD/NASH phenotype. We could not exclude a possible synergic effect of *Osr1*-overexpression in various cell types (especially hepatocytes) on protecting NAFLD/NASH, although we showed that deleting hepatic *Osr1* did not change the NAFLD/NASH progression. Targeting PPAR γ , rosiglitazone treatment blocked NAFLD/NASH progression and improved insulin sensitivity, consistent with previous reports.^{32,33} Rosiglitazone acts on many cells, including adipocytes, hepatocytes, and macrophages. The *Osr1* ^{$\Delta M\phi$} mice showed reduced body weight gain upon rosiglitazone, possibly because of the effects on adipocytes²⁴; however, inhibited body weight gain was not observed in the rosiglitazone treated *Osr1*^F mice that also improved NASH. The therapeutic effects of rosiglitazone to reduce hepatic steatosis may be offset by their actions to enhance PPAR γ expression on hepatocyte function.³² Thus, the amelioration of NAFLD in our study highlights a working mechanism of rosiglitazone targeting macrophage-mediated inflammation and insulin sensitization. Our findings suggest a promising treatment for NASH by targeting the macrophage-centered inflammation mediated by the *Osr1*-PPAR γ axis.

Materials and Methods

Human Liver Samples

De-coded human liver samples came from the Tongji Hospital, Huazhong University of Science and Technology (Wuhan, China). The *Osr1* immunohistochemistry staining was performed at the clinical pathology laboratory of Tongji Hospital (Wuhan, China).

Animals and Treatments

The *Osr1*^{fl/fl} mice were generated as described.^{34,35} Mice were maintained in a C57BL/6 background on a 12-hour light/dark cycle. Hepatocyte and myeloid cell-specific *Osr1*-disrupted mice were generated using the Cre-LoxP strategy. Briefly, control *Osr1*^{fl/+} or *Osr1*^{fl/fl} (*Osr1*^F), heterozygous *Alb*^{Cre+}*Osr1*^{fl/+} (*Osr1* ^{$\Delta Hep/+$}) and *LysM*^{cre/+}*Osr1*^{fl/+} (*Osr1* ^{$\Delta M\phi/+$}), and homozygous *Alb*^{Cre+}*Osr1*^{fl/fl} (*Osr1* ^{ΔHep}) and *LysM*^{cre/+}*Osr1*^{fl/fl} (*Osr1* ^{$\Delta M\phi$}) mice were treated with regular chow diet, HFD (60% fat calories, 14 weeks), MCD (4 weeks) or Western diet (WD, 40% fat calories, 20% fructose and 2% cholesterol, 20 weeks) at the age of 8 weeks. STAM models were induced by a single subcutaneous injection of 200 μ g streptozocin (Sigma) 2 days after birth and feeding with HFD for 4 weeks.

In a separate experiment, male *Osr1*^F or *Osr1* ^{$\Delta M\phi$} mice were given daily intraperitoneal injections of either vehicle (dimethyl sulfoxide) or rosiglitazone (10 mg/kg/day) for 4 weeks after 10 weeks of HFD treatment. For the in vivo AAV rescue study, mice were treated with pAAV8L-control or

pAAV8L-*Osr1* through the retro-orbital venous sinus at wean, followed by 14 weeks of HFD or 4 weeks of MCD. All animal experiments were completed according to the protocols reviewed and approved by the Institutional Animal Care and Use Committee of Texas A&M University.

Intraperitoneal Glucose Tolerance Test

Mice were fasted overnight by transferring them to clean cages with no food in the upper or bottom sections of the cage. Mice were weighed and injected intraperitoneally with 20% glucose solution (2 g/kg body weight glucose). Blood from the tail vein was obtained at 0, 15, 30, 60, 90, and 120 minutes after the injection to determine blood glucose level with a glucose meter.

RNA Sequencing

RNA quantification was performed on a bioanalyzer (Agilent Technologies, Santa Clara, CA). One nanogram was used as input for library preparation using Nextera XT DNA Library Prep Kit (Illumina, San Diego, CA) and Nextera XT Index Kit (Illumina, San Diego, CA). Libraries were quantified, normalized to 4 nM, pooled, and diluted to be sequenced on a NextSeq (Illumina) using 75 bp paired-end sequencing.

Real-time PCR

qPCR was performed using SYBR Green Supermix (Bio-Rad, Hercules, CA) on the CFX384 real-time system (Bio-Rad). After the cycling program, melting curve analysis was performed immediately after amplification to confirm primer specificity. Three or more biological replicates were used for each condition, and 2 technical replicates were performed for each sample. Quantification data were analyzed using methods derived from the comparative CT method. For gene expression analysis, genes of interest were normalized to *Cyclophilin*, and data were expressed as fold change against *Cyclophilin* (\pm standard error of the mean).

Fluorescence Lifetime Imaging of Macrophages and Imaging Processing

The NAD(P)H and FAD fluorescence lifetime images of macrophages were acquired using an inverted multi-photon fluorescence microscopy (Marianas, 3i) coupled to a 40X water-immersion objective (1.1 NA). NAD(P)H and FAD fluorescence were stimulated at 750 nm and 890 nm, respectively, using a titanium:sapphire femtosecond laser (COHERENT, Chameleon). The laser power was set at 16 mW for NAD(P)H fluorescence excitation and 30 mW for FAD fluorescence excitation; 400- to 480-nm and 500- to 580-nm bandpass filters were used to isolate NAD(P)H and FAD fluorescence, respectively. Two photomultiplier tubes (Hamamatsu) were used to detect the fluorescence for each channel. Fluorescence lifetime images were obtained using time-correlated single-photon counting electrons (SPC-150N, Becker, and Hickl). Each 256 \times 256-pixel fluorescence lifetime image was obtained with a pixel dwell time of

50 μ s and 5 frame repeats. The instrument response function was measured using the NAD(P)H channel from the second harmonic generation of urea crystals excited at 900 nm.

The fluorescence lifetime analysis was performed using SPCImage (Becker and Hickl). Fluorescence lifetime components were obtained by deconvolving the instrument response function and fitting the decay result to a 2-component exponential decay model ($I(t) = \alpha_1 e^{-t/\tau_1} + \alpha_2 e^{-t/\tau_2} + C$), where $I(t)$ is the fluorescence intensity as a function of time t , τ_1 and τ_2 are the short and long lifetimes, respectively, α_1 and α_2 are their corresponding fractions ($\alpha_1 + \alpha_2 = 1$), and C accounts for the background noise. To obtain the lifetime values of each cell, cell masks were generated by segmenting NAD(P)H intensity images into individual cells using a semi-automated pipeline in CellProfiler. A mean fluorescence lifetime ($\tau_m = \alpha_1 \tau_1 + \alpha_2 \tau_2$), lifetime redox ratio (NAD(P)H $\alpha_2/\text{FAD } \alpha_1$), and mean lifetime component values for each cell were calculated in MATLAB based on the cell masks.

Statistical Analysis

Data were expressed as means \pm standard deviations or means \pm standard errors. Statistical significance was assessed using the unpaired, 2-tailed Student t tests or one-way analysis of variance. Significant difference was indicated as: * $P < .05$; ** $P < .01$; and *** $P < .001$.

References

1. Younossi ZM, Blissett D, Blissett R, Henry L, Stepanova M, Younossi Y, Racila A, Hunt S, Beckerman R. The economic and clinical burden of nonalcoholic fatty liver disease in the United States and Europe. *Hepatology* 2016;64:1577–1586.
2. Younossi Z, Anstee QM, Marietti M, Hardy T, Henry L, Eslam M, George J, Bugianesi E. Global burden of NAFLD and NASH: trends, predictions, risk factors and prevention. *Nat Rev Gastroenterol Hepatol* 2018; 15:11–20.
3. Siegel AB, Zhu AX. Metabolic syndrome and hepatocellular carcinoma: two growing epidemics with a potential link. *Cancer* 2009;115:5651–5661.
4. Younossi ZM, Koenig AB, Abdelatif D, Fazel Y, Henry L, Wymer M. Global epidemiology of nonalcoholic fatty liver disease—Meta-analytic assessment of prevalence, incidence, and outcomes. *Hepatology* 2016;64:73–84.
5. Estes C, Anstee QM, Arias-Loste MT, Bantel H, Bellantani S, Caballeria J, Colombo M, Craxi A, Crespo J, Day CP, Eguchi Y, Geier A, Kondili LA, Kroy DC, Lazarus JV, Loomba R, Manns MP, Marchesini G, Nakajima A, Negro F, Petta S, Ratziu V, Romero-Gomez M, Sanyal A, Schattenberg JM, Tacke F, Tanaka J, Trautwein C, Wei L, Zeuzem S, Razavi H. Modeling NAFLD disease burden in China, France, Germany, Italy, Japan, Spain, United Kingdom, and United States for the period 2016–2030. *J Hepatol* 2018; 69:896–904.
6. Machado MV, Diehl AM. Pathogenesis of nonalcoholic steatohepatitis. *Gastroenterology* 2016;150:1769–1777.
7. Buzzetti E, Pinzani M, Tsochatzis EA. The multiple-hit pathogenesis of non-alcoholic fatty liver disease (NAFLD). *Metabolism* 2016;65:1038–1048.
8. Jindal A, Bruzzi S, Sutti S, Locatelli I, Bozzola C, Paternostro C, Parola M, Albano E. Fat-laden macrophages modulate lobular inflammation in nonalcoholic steatohepatitis (NASH). *Exp Mol Pathol* 2015; 99:155–162.
9. Viola A, Munari F, Sanchez-Rodriguez R, Scolaro T, Castegna A. The metabolic signature of macrophage responses. *Front Immunol* 2019;10:1462.
10. Odegaard JI, Ricardo-Gonzalez RR, Red Eagle A, Vats D, Morel CR, Goforth MH, Subramanian V, Mukundan L, Ferrante AW, Chawla A. Alternative M2 activation of Kupffer cells by PPAR δ ameliorates obesity-induced insulin resistance. *Cell Metab* 2008;7:496–507.
11. Coulter DE, Swaykus EA, Beran-Koehn MA, Goldberg D, Wieschaus E, Schedl P. Molecular analysis of odd-skipped, a zinc finger encoding segmentation gene with a novel pair-rule expression pattern. *EMBO J* 1990; 9:3795–3804.
12. Zhang KK, Xiang M, Zhou L, Liu J, Curry N, Suner DH, Garcia-Pavia P, Zhang X, Wang Q, Xie L. Gene network and familial analyses uncover a gene network involving Tbx5/Osr1/Pcsk6 interaction in the second heart field for atrial septation. *Hum Mol Genet* 2016;25:1140–1151.
13. Wang Q, Lan Y, Cho ES, Maltby KM, Jiang R. Odd-skipped related 1 (Odd 1) is an essential regulator of heart and urogenital development. *Dev Biol* 2005; 288:582–594.
14. Zhang Y, Yuan Y, Liang P, Guo X, Ying Y, Shu XS, Gao M Jr, Cheng Y. OSR1 is a novel epigenetic silenced tumor suppressor regulating invasion and proliferation in renal cell carcinoma. *Oncotarget* 2017;8:30008–30018.
15. Zhao J, Liang Q, Cheung KF, Kang W, Lung RWM, Tong JHM, To KF, Sung JJY, Yu J. Genome-wide identification of Epstein-Barr virus-driven promoter methylation profiles of human genes in gastric cancer cells. *Cancer* 2013;119:304–312.
16. Zong L, Sun Y. OSR1 suppresses acute myeloid leukaemia cell proliferation by inhibiting LGR5-mediated JNK signalling. *Autoimmunity* 2021;54:561–568.
17. Zhou Y, Liu Z, Lynch EC, He L, Cheng H, Liu L, Li Z, Li J, Lawless L, Zhang KK, Xie L. Osr1 regulates hepatic inflammation and cell survival in the progression of non-alcoholic fatty liver disease. *Lab Invest* 2021; 101:477–489.
18. Lynch EC, Liu Z, Liu L, Wang X, Zhang KK, Xie L. Disrupting Osr1 expression promoted hepatic steatosis and inflammation induced by high-fat diet in mouse model. *PLoS One* 2022;17:e0268344.
19. Pellicoro A, Ramachandran P, Iredale JP, Fallowfield JA. Liver fibrosis and repair: immune regulation of wound healing in a solid organ. *Nat Rev Immunol* 2014; 14:181–194.
20. Hu L, Wang N, Cardona E, Walsh AJ. Fluorescence intensity and lifetime redox ratios detect metabolic

- perturbations in T cells. *Biomed Opt Express* 2020; 11:5674–5688.
21. Zhou L, Liu J, Olson P, Zhang K, Wynne J, Xie L. Tbx5 and *Osr1* interact to regulate posterior second heart field cell cycle progression for cardiac septation. *J Mol Cell Cardiol* 2015;85:1–12.
 22. Zhang Z, Iglesias D, Eliopoulos N, El Kares R, Chu LL, Romagnani P, Goodyer P. A variant *OSR1* allele which disturbs *OSR1* mRNA expression in renal progenitor cells is associated with reduction of newborn kidney size and function. *Hum Mol Genet* 2011;20:4167–4174.
 23. Jung SH, Evans CJ, Uemura C, Bannerjee U. The *Drosophila* lymph gland as a developmental model of hematopoiesis. *Development* 2005;132:2521–2533.
 24. Odegaard JI, Ricardo-Gonzalez RR, Goforth MH, Morel CR, Subramanian V, Mukundan L, Red Eagle A, Vats D, Brombacher F, Ferrante AW, Chawla A. Macrophage-specific PPAR γ controls alternative activation and improves insulin resistance. *Nature* 2007; 447:1116–1120.
 25. Luo W, Xu Q, Wang Q, Wu H, Hua J. Effect of modulation of PPAR- γ activity on Kupffer cells M1/M2 polarization in the development of non-alcoholic fatty liver disease. *Sci Rep* 2017;7:44612.
 26. Pello OM, De Pizzol M, Mirolo M, Soucek L, Zammataro L, Amabile A, Doni A, Nebuloni M, Swigart LB, Evan GI, Mantovani A, Locati M. Role of c-MYC in alternative activation of human macrophages and tumor-associated macrophage biology. *Blood* 2012; 119:411–421.
 27. Liu Y, Xu R, Gu H, Zhang E, Qu J, Cao W, Huang X, Yan H, He J, Cai Z. Metabolic reprogramming in macrophage responses. *Biomark Res* 2021;9:1.
 28. Vats D, Mukundan L, Odegaard JI, Zhang L, Smith KL, Morel CR, Wagner RA, Greaves DR, Murray PJ, Chawla A. Oxidative metabolism and PGC-1 β attenuate macrophage-mediated inflammation. *Cell Metab* 2006;4:13–24.
 29. Korbecki J, Bajdak-Rusinek K. The effect of palmitic acid on inflammatory response in macrophages: an overview of molecular mechanisms. *Inflamm Res* 2019;68:915–932.
 30. Kratz M, Coats BR, Hisert KB, Hagman D, Mutskov V, Peris E, Schoenfelt KQ, Kuzma JN, Larson I, Billing PS, Landerholm RW, Crouthamel M, Gozal D, Hwang S, Singh PK, Becker L. Metabolic dysfunction drives a mechanistically distinct proinflammatory phenotype in adipose tissue macrophages. *Cell Metab* 2014; 20:614–625.
 31. Bae S, Park PSU, Lee Y, Mun SH, Giannopoulou E, Fujii T, Lee KP, Violante SN, Cross JR, Park-Min KH. MYC-mediated early glycolysis negatively regulates proinflammatory responses by controlling IRF4 in inflammatory macrophages. *Cell Rep* 2021;35:109264.
 32. Ratziu V, Charlotte F, Bernhardt C, Giral P, Halbron M, Lenaour G, Hartmann-Heurtier A, Bruckert E, Poynard T; LIDO Study Group. Long-term efficacy of rosiglitazone in nonalcoholic steatohepatitis: results of the fatty liver improvement by rosiglitazone therapy (FLIRT 2) extension trial. *Hepatology* 2010;51:445–453.
 33. Bouhlef MA, Derudas B, Rigamonti E, Dievarat R, Brozek J, Haulon S, Zawadzki C, Jude B, Torpier G, Marx N, Saels B, Chinetti-Gbaguidi G. PPAR γ activation primes human monocytes into alternative M2 macrophages with anti-inflammatory properties. *Cell Metab* 2007;6:137–143.
 34. Lan Y, Liu H, Ovitt CE, Jiang R. Generation of *Osr1* conditional mutant mice. *Genesis* 2011;49:419–422.
 35. Liu H, Lan Y, Xu J, Chang CF, Brugmann SA, Jiang R. Odd-skipped related-1 controls neural crest chondrogenesis during tongue development. *Proc Natl Acad Sci U S A* 2013;110:18555–18560.
-
- Received June 28, 2022. Accepted December 16, 2022.**
- Correspondence**
Address correspondence to: Linglin Xie, MD, PhD, Department of Nutrition, Texas A&M University, College Station, TX 77845. e-mail: linglin.xie@tamu.edu.
- CRedit Authorship Contributions**
Lin Liu, MD, PhD (Conceptualization: Equal; Data curation: Lead; Formal analysis: Lead; Investigation: Lead; Methodology: Lead; Software: Lead; Writing – original draft: Lead; Writing – review & editing: Lead)
Yi Zhou, MD, PhD (Data curation: Supporting)
Zhimin Liu, MD, PhD (Data curation: Supporting; Investigation: Supporting)
Jiangyuan Li, Graduate Student (Data curation: Supporting; Methodology: Supporting; Software: Supporting)
Linghao Hu, Graduate Student (Data curation: Supporting; Investigation: Supporting)
Leya He, MD, PhD (Data curation: Supporting)
Guannan Gao, MS (Data curation: Supporting)
Brian Kidd, Graduate Student (Data curation: Supporting)
Alexandra Walsh, PhD (Data curation: Supporting; Validation: Supporting; Writing – original draft: Supporting; Writing – review & editing: Supporting)
Rulang Jiang, PhD (Resources: Supporting; Writing – original draft: Supporting; Writing – review & editing: Supporting)
Chaodong Wu, MD, PhD (Resources: Supporting; Writing – original draft: Supporting; Writing – review & editing: Supporting)
Ke Zhang, PhD (Data curation: Supporting; Formal analysis: Supporting; Writing – original draft: Supporting; Writing – review & editing: Supporting)
Linglin Xie, MD, PhD (Conceptualization: Lead; Formal analysis: Supporting; Funding acquisition: Lead; Investigation: Lead; Project administration: Lead; Supervision: Lead; Validation: Lead; Writing – original draft: Supporting; Writing – review & editing: Supporting)
- Conflicts of interest**
The authors disclose no conflicts.
- Funding**
This project is supported by a National Institutes of Health R01 grant (1R01DK112368-01, PI: Linglin Xie).